ACS Catalysis

pubs.acs.org/acscatalysis Research Article

Tailoring the Interfacial Water Structure by Electrolyte Engineering for Selective Electrocatalytic Reduction of Carbon Dioxide

Nandita Mohandas, Tharangattu N. Narayanan,* and Angel Cuesta*

Cite This: *ACS Catal.* 2023, 13, 8384−8393 Read Online

ACCESS | Metrics & More | Article Recommendations | Supporting Information

ABSTRACT: Engineering aqueous electrolytes with low amounts of additives to achieve a tunable CO_2 reduction product is an underexplored territory in electrocatalysis. Here, we show the enhancement of the Faradaic efficiency (FE) of CO_2 reduction to CO on unmodified polycrystalline gold from ∼67 to ∼94% by the addition of up to 15 mol % of *N*,*N*-dimethylformamide (DMF) to an aqueous electrolyte. The role of electrolyte structure modification near the electrode−electrolyte interface was studied using *in situ* surface-enhanced infrared absorption spectroscopy in attenuated total reflection mode (ATR-SEIRAS). In addition to the expected detection of the adsorbed CO (CO_{ad}) intermediate present on the Au surface, in both the linearly bonded and bridge-bonded forms, we observed changes in the structure of interfacial water induced by the addition of DMF. The changes in the water stretching band and the DMF carbonyl band indicate an increase in the strongly hydrogen-bonded DMF−water pairs with increasingly negative potential near the interface in the presence of DMF. We hold this interfacial water structure modification by DMF responsible for increasing the CO2RR FE and decreasing the competing hydrogen evolution reaction (HER). Furthermore, the suppression of the HER is observed in other electrolytes and also when platinum was used as an electrode and hence can be a potential method for increasing the product selectivity of complex electrocatalytic reactions.

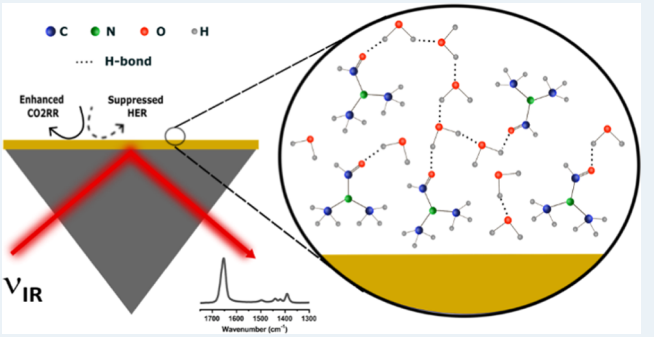

KEYWORDS: *electrochemical CO_2 reduction, electrolyte engineering, hydrogen-bonding network, ATR-SEIRAS, DMF, CO2RR product selectivity, HER suppression, spectro-electrochemistry*

1. INTRODUCTION

Engineering electrolytes for tunable heterogeneous electron transfer processes is an emerging research focus for selective product formation. Such engineering can be accomplished with both aqueous and nonaqueous electrolytes, where the thermodynamics and kinetics of the reaction processes can be modified.[1−4] Among different electrochemical processes that could benefit from electrolyte engineering is the electrochemical CO_2 reduction reaction (CO2RR), one of the most promising approaches to developing a circular economy.[5,6] This is because CO_2 is an abundant carbon source, and so processing it electrochemically does not harm the environment and can, in fact, help to decrease the carbon footprint of various processes. However, steering the reaction toward the desired products represents a fundamentally important challenge in electrochemistry.[5,7−9]

The standard equilibrium potential to form most CO2RR products is similar to that for the hydrogen evolution reaction (HER) in aqueous electrolytes.[8−10] Therefore, the electrochemical CO2RR in aqueous electrolytes usually competes with the HER, and it is therefore important to design routes to suppress the latter, while allowing the former to proceed with high current efficiencies. Understanding how to control the relative activities of the HER and CO2RR is cardinal for improving the selectivity toward CO2RR.

Most of the research in the field of CO2RR has focused on the development of electrocatalytic materials and on understanding the impact of catalyst morphology on the reaction. An equally important role in the CO2RR is played, though, by the electrolyte.[1,2,11] However, the role of the electrolyte in the CO2RR has been comparatively less explored. Depending on the species in the electrolyte, the structure of the electrode−electrolyte interface, the adsorption and stability of intermediates, the concentration of CO_2 at the surface, and the viscosity and conductivity of the electrolyte can be influenced. Using additives can be a promising strategy to enhance the CO2RR in aqueous electrolytes since the advantages of both

Received: March 17, 2023
Revised: May 19, 2023

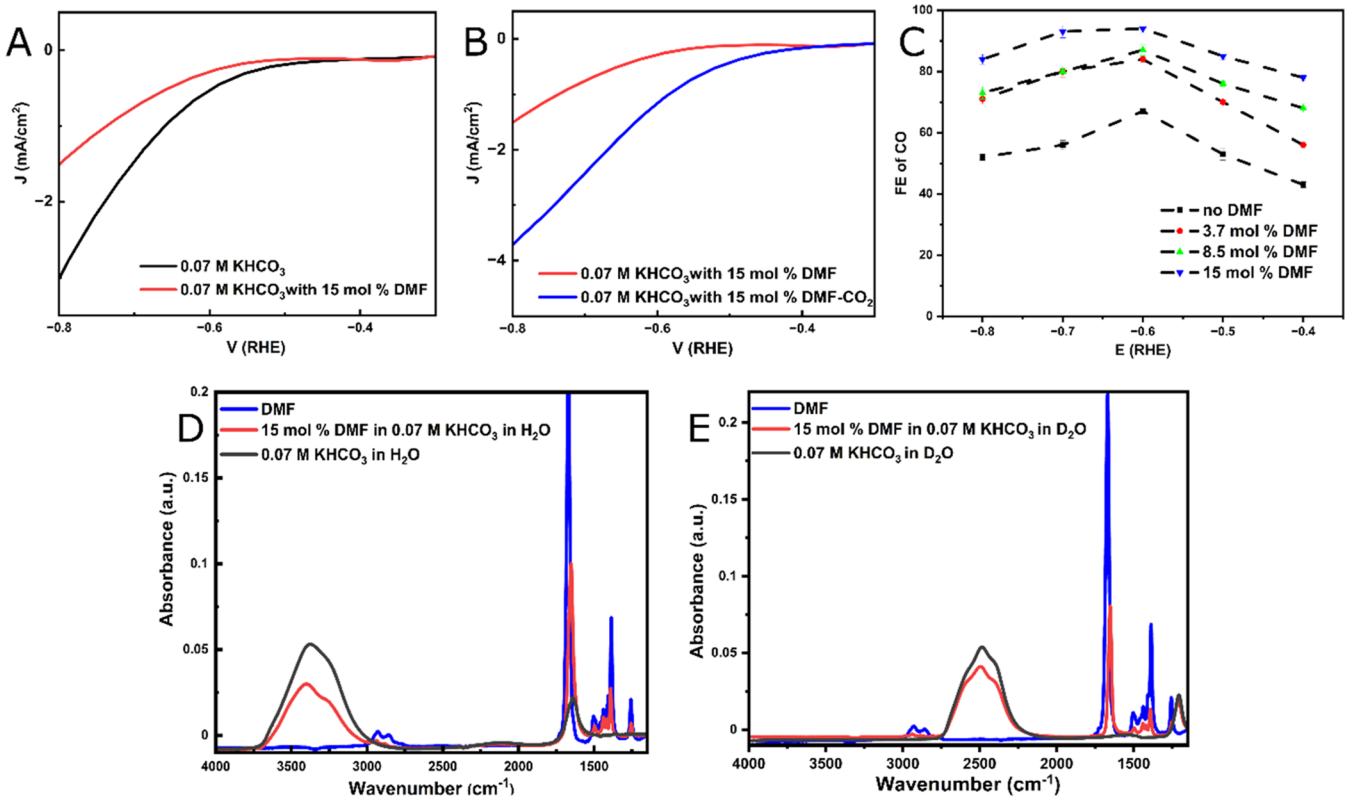

Figure 1. (A) LSVs of Au in 0.07 M $KHCO_3$ with (red line) and without (black line) 15 mol % DMF. (B) LSVs of Au in 0.07 M $KHCO_3$ with 15 mol % DMF in Ar- (red line) and CO_2-saturated (blue line) conditions. (C) Faradaic efficiency of CO formation as a function of potential for different mol % of DMF (the dashed lines are just a guide to the eye). (D, E) ATR infrared absorbance spectra of DMF (blue lines) and of 0.07 M $KHCO_3$ solutions in H_2O (D) and in D_2O (E) in the presence (red lines) and absence (black lines) of 15 mol % DMF.

additive and aqueous electrolytes can be simultaneously achieved.[1]

Ionic additives including organic salts,[12] surfactants,[13−15] and ionic liquids[16−18] have been used to enhance the CO2RR in aqueous electrolytes. Neubauer et al.[16] studied the effect of the concentration of the ionic liquid (IL) 1-ethyl-3-methylimidazolium trifluoromethanesulfonate ([EMIM]-[OTF]) (0−50 mol %) in 10 mM $KHCO_3$ on the CO2RR on silver. They reported that a significant CO_2 reduction was obtained for electrolytes with more than 20% IL, which when increased to 50% leads to a Faradaic efficiency (FE) of 95.6% for CO. They attributed this observation to blocking H_2O diffusion to the surface at high IL concentrations. In another study, Dong et al.[19] showed that the strong solvation effect at high concentrations (15−21 M) of lithium bis-(trifluoromethanesulfonyl)imide (LiTFSI) locks down the H_2O molecules to behave drastically different from bulk H_2O. They showed that the H_2O reduction activity greatly reduced (which they showed can be only partially attributed to the decreased chemical potential of H_2O), increasing the FE of CO_2 reduction activity and leading to a high selectivity toward CO production, up to 80%. But these high concentration systems are not easily achievable, are difficult to probe, and are not economically feasible.

Although most of the additives used in heterogeneous CO2RR have an ionic nature, nonionic organic additives such as primary amines and pyridine have also been employed to enhance the CO2RR.[20−22] Nitrogen-containing heterocyclic compounds such as pyridine have been reported to decrease the overpotential and promote the CO2RR.

It has been shown that *N*,*N*-dimethylformamide (DMF) enhances the H-bonding network of water when the volume fraction of DMF in the solution is less than 0.4. However, a further increase in the DMF concentration in the solution could lead to a breakdown of the water network.[23,24] Some recent reports indicate that addition of DMF in aqueous electrolytes can tune the H-bonding effect between water and DMF, thereby leading to better battery performance.[25,26] As shown by Chen and co-workers,[26] upon introducing 30% (volume fraction) DMF to the aqueous electrolyte, the preferential hydrogen-bonding effect between DMF and H_2O effectively reduces the bulk water activity and hinders deprotonation of the electrolyte, thereby boosting the Zn anode reversibility. But, since the interface can be largely different from the bulk electrolyte, a detailed understanding of the electrode−electrolyte interface modification due to the electrolyte engineering and its impact on the heterogeneous electron transfer process is still unclear.

In this report, we discuss this DMF−water hybrid solvent system for electrochemical CO2RR. Au is used as a prototypical catalyst platform in our studies. We used potassium bicarbonate ($KHCO_3$) as the electrolyte, as is common in CO2RR due to its buffer capacity and low cost. With 15 mol % of DMF in 0.07 M $KHCO_3$, we could achieve a Faradaic efficiency (FE) of ∼94% for CO2RR to CO on a bare unmodified polycrystalline gold catalyst, whereas for pure 0.07 M $KHCO_3$ with no DMF, the FE was only ∼67%. Since the CO2RR (indeed, all electrochemical reactions) is an interfacial process, a deep understanding of the electrode−electrolyte interface is crucial. Infrared spectroscopy has become an

https://doi.org/10.1021/acscatal.3c01223
ACS Catal. 2023, 13, 8384−8393

indispensable tool in electrochemistry, particularly in electrocatalysis, since it allows *in situ*, nondestructive, and label-free analysis of species at the electrode−electrolyte interface.[27] We conducted *in situ* studies of the electrochemical interface under investigation using surface-enhanced infrared spectroscopy in the attenuated total reflection mode (ATR-SEIRAS). From the studies, we could analyze that DMF as an additive in the electrolyte can tailor the H-bonding network of water, which is responsible for the suppression of the competing HER. Our study throws light in the direction of the importance of the interfacial water structure modification through simple electrolyte engineering for selective CO2RR.

2. EXPERIMENTAL SECTION

ATR-SEIRA spectra were collected with the potential being stepped down from 0 to −1.6 V vs Ag/AgCl (KCl_{sat}) using a Nicolet iS50R FTIR spectrometer equipped with a liquid N_2-cooled MCT detector and a home-made ATR accessory, using unpolarized light. Each spectrum consisted of 120 interferograms with a spectral resolution of 8 cm^{-1}. The background spectrum also consisted of 120 interferograms and was taken at the potential indicated in the corresponding figure caption. Spectra were calculated in absorbance units as $A = -\log \frac{R_{sample}}{R_{background}}$, where $R_{background}$ and R_{sample} are the reference and sample spectra, respectively. An EmStat3 Potentiostat from PalmSens was used to control the potential of our working electrode and measure the current flowing through it during the ATR-SEIRAS experiments. The working electrode was a gold film deposited on the totally reflecting plane of a Si prism beveled at 60° following the method mentioned in the Supporting Information. The gold-coated Si prism was attached to the spectro-electrochemical cell using an O-ring seal, and electrical contact with the film was made by pressing onto it a circular gold wire. Before any IR measurements, the film was cycled in the corresponding electrolyte to check its stability, clean the surface, and obtain a reproducible surface morphology. A gold mesh was used as a counter electrode and a leak-proof Ag/AgCl (KCl_{sat}) electrode was used as a reference electrode. However, all of the potentials in the text are referred to the RHE scale, unless otherwise stated.

Further experimental details (chemicals used, electrochemical measurements, and gas chromatography) are presented in the Supporting Information.

3. RESULTS AND DISCUSSION

We employed Au as a model catalyst for this study, as it shows high selectivity toward the production of CO as opposed to other carbonaceous products.[8] Hence, HER suppression should result in an increase in the CO production. Detailed bulk electrochemical studies were conducted, as discussed in Section 2, and the products formed after 30 min of electrolysis were analyzed. To verify the HER suppression hypothesis, we conducted electrochemical studies with the addition of DMF to our electrolyte using linear sweep voltammetry (LSV). The onset of hydrogen evolution in 0.07 M $KHCO_3$ shifts negatively when 15 mol % of DMF was added to the electrolyte (Figure 1A). We could not increase the DMF concentration further due to the poor solubility of $KHCO_3$ in DMF. This DMF-induced suppression of the HER is not limited to $KHCO_3$ solutions and was also observed in 0.07 M KOH and 0.07 M H_2SO_4 (Figure S1). We also observed DMF-induced suppression of the HER with polycrystalline Cu, Ag, and Pt electrodes in different electrolytes when 15 mol % of DMF was added (Figures S2 and S3). Hence, it is reasonable to conclude that the suppression of the HER in aqueous electrolytes in the presence of DMF is universal.

Saturation with CO_2 in the 0.07 M $KHCO_3$ electrolyte resulted in a higher negative current density starting at a less negative potential in comparison to the corresponding LSV conducted in an Ar-purged electrolyte, both in the presence and in the absence of 15 mol % of DMF (Figure 1A,B). Although this increase in the cathodic current may be attributed to the CO2RR, it is necessary to verify that a lower pH at the interface, due to the buffering effect in the CO_2-saturated solution, is not behind the less negative onset of hydrogen evolution and the higher current at any given potential beyond the onset. As can be seen, the addition of DMF has a larger effect on the current in Ar-saturated (black line in Figure 1A and red line in Figure 1B) than in CO_2-saturated 0.07 M $KHCO_3$ (red line in Figure 1A and blue line in Figure 1B). Because the buffering effect of CO_2 must be very similar whether DMF is present or not and the inhibition of the HER by DMF must be similar in Ar- and CO_2-saturated solutions, the difference between the Ar- and CO_2-saturated solutions in the presence of DMF must be due to the contribution of the CO2RR. In other words, the changes observed in the LSVs in Figure 1 under saturation with CO_2 must be due at least partly to the CO2RR. This is confirmed by the analysis of the reaction products after electrolysis by gas chromatography (see below).

To quantify the products formed and understand the main contributions to the cathodic current, we performed potentiostatic electrolysis and simultaneous product analysis using gas chromatography. Only CO and H_2 were detected as products of the reaction. No effect on the morphology of the electrode surface could be observed using SEM (Figure S4) and no liquid products or decomposition of the electrolyte by NMR (Figure S5). The Faradaic efficiency (FE) of CO formation as a function of the potential applied during electrolysis is presented in Figure 1C for DMF-free $KHCO_3$ (black squares) and for different concentrations of DMF (red circles, green triangles, and blue triangles). The Faradaic efficiencies and partial current densities of CO and H_2 are tabulated in Table S1. The CO FE in DMF-free 0.07 M $KHCO_3$ is relatively poor, with a maximum of ∼67% at −0.6 V. We saw that the selectivity for CO increases with increasing mol % of DMF. The maximum FE for CO was ∼94% in 15 mol % DMF at −0.6 V, with a current density of 1.6 mA cm^{-2}. We only analyzed the potential window between −0.4 and −0.8 V because, at higher overpotentials, mass-transport limitations and CO_2 depletion at the interface due to the high local pH favor the HER over the CO2RR.[8,22]

Although the addition of DMF changes the bulk pH of the electrolyte, as shown in Table S2 these changes are similar to those expected at the interface during the HER and CO2RR. Moreover, DMF increases the pH, which should decrease the CO FE by reducing the availability of CO_2 at the interface, while we observe exactly the opposite effect.

To understand the mechanism behind the enhanced CO FE as a result of the electrolyte engineering and analyze changes to the structure of the bulk electrolyte brought about by the addition of DMF, we used attenuated total reflectance infrared (ATR-IR) absorption spectroscopy (Figure 1D,E) and ^1H nuclear magnetic resonance (NMR) spectroscopy (Figure S6).

https://doi.org/10.1021/acscatal.3c01223
ACS Catal. 2023, 13, 8384−8393

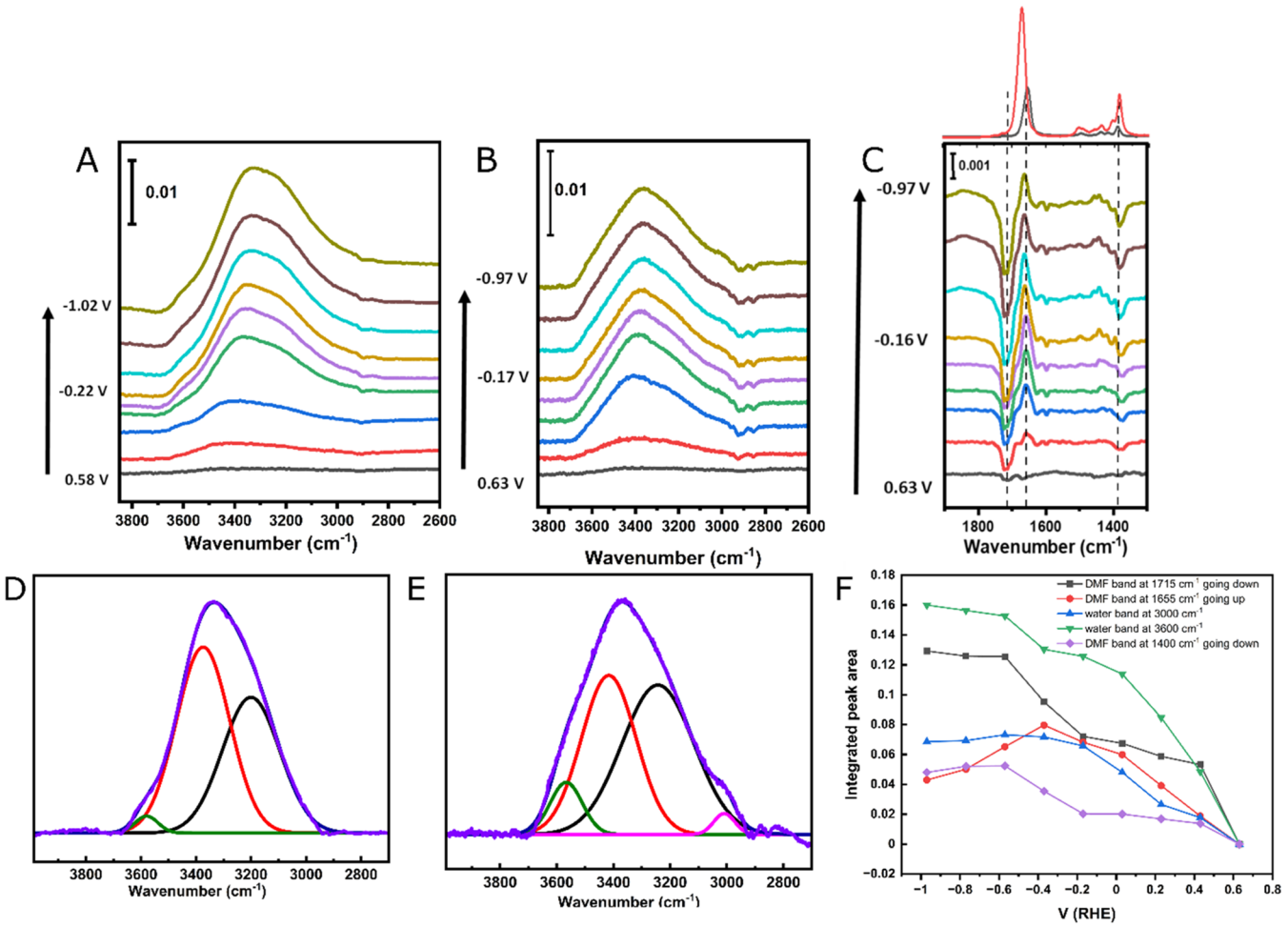

Figure 2. *In situ* ATR-SEIRA spectra in the O−H stretching region at different applied potentials in DMF-free 0.07 M $KHCO_3$ (A) and in 0.07 M $KHCO_3$ containing 15 mol % DMF (B). *In situ* ATR-SEIRA spectra in 0.07 M $KHCO_3$ with 15 mol % DMF in D_2O as a function of the applied potential in the spectral region corresponding to the carbonyl mode of DMF (C). The potential interval between spectra is 0.2 V. The spectra of pure DMF (red line) and of 15 mol % DMF in water (black line) are shown on top of panel (C) for comparison. Deconvolution of the O−H stretching band at −0.62 V in DMF-free 0.07 M $KHCO_3$ (D) and at −0.57 V in 0.07 M $KHCO_3$ containing 15 mol % DMF (E). The evolution with the applied potential of the integrated intensity of the DMF C═O stretching bands at 1715 and 1655 cm^{-1}, the components at 3000 and 3600 cm^{-1} of the water O−H stretching band, and the DMF methyl deformation band at 1400 cm^{-1} (for those bands with negative absorption in panel (C), the negative of the integrated absorption has been plotted) is shown in panel (F).

Surface-enhanced infrared absorption spectroscopy in the attenuated total reflection mode (ATR-SEIRAS) was used to analyze the effect of the addition of DMF on the structure of the electrode−electrolyte interface and its dependence on the applied potential.

As expected, the chemical shift of the protons of water appears at ∼4.70 ppm (Figure S6). Addition of 15 mol % of DMF to the solution results in a new signal for the protons of water shifted downfield to 4.76 ppm. This suggests a lower percentage of hydrogen bond-free water.[28] Similarly, the downfield shift of the proton bonded to the carbon atom of the carbonyl group of DMF was also suggestive of higher degree of the H-bond network in the solution (Figure S6).[26]

Bulk IR absorption spectra of the electrolytes are shown in Figure 1D,E. The spectrum of pure DMF (blue traces in Figure 1D,E) has a prominent peak at 1676 cm^{-1} corresponding to the C−O stretching of the amide group. The peaks in the 2850−2920 cm^{-1} region correspond to the symmetric and asymmetric C−H stretching modes of the methyl groups and of the C−H bond of the carbonylic carbon, the peak around 1500 cm^{-1} contains the contribution of the amidic C−N stretching, and the bands at 1440 and 1409 cm^{-1} correspond to the asymmetric and symmetric bending, respectively, of the CH_3 groups. The band around 1270 cm^{-1} corresponds to the asymmetric N−CH_3 stretching.[29] In the absence of DMF, aqueous 0.07 M $KHCO_3$ solutions show the typical water bending mode at 1645 cm^{-1} and the broad band corresponding to the O−H stretching of water at 3200−3600 cm^{-1} (black trace in Figure 1D). When 15 mol % DMF is added to the aqueous $KHCO_3$ solution (red trace in Figure 1D), the water peak at 1640 cm^{-1} and the DMF peak at 1676 cm^{-1} overlap in a single peak around 1650 cm^{-1}, which makes the analysis of potential changes in the bulk water structure of the electrolyte difficult. This can be solved by substituting D_2O for H_2O, as the D−O−D bending of D_2O red-shifts to 1205 cm^{-1} (black trace in Figure 1E). Although the effect of the presence of DMF on the D−O−D bending mode of D_2O is negligible, the interaction of DMF with water in 15 mol % DMF in 0.07 M $KHCO_3$ red-shifts the amide carbonyl peak to 1654 cm^{-1}. This red shift can be attributed to the increase in the effective mass of the C−O stretching mode due to H-

https://doi.org/10.1021/acscatal.3c01223
ACS Catal. 2023, 13, 8384−8393

bonding between the oxygen of the DMF carbonyl group and water.

The addition of DMF results mainly in a decrease in the intensity of the water stretching bands at 3200−3600 cm^{-1} (in H_2O) and 2200−2700 cm^{-1} (in D_2O), without significant changes in their shapes. But the bulk and interfacial electrolyte structures can show stark contrast; hence, understanding and comprehending the interfacial electrolyte structure as a function of potential can give us a clear picture of the effect of DMF on modifying the electrochemical interface at potentials relevant for the CO2RR. The interfacial structure of the electrolyte was probed by *in situ* ATR-SEIRAS (Figure 2) to gain insights about the potential-induced accumulation/depletion and reorientation of water and DMF, as well as the adsorption and desorption of intermediates and spectators.[27,30−33]

The cyclic and the linear sweep voltammograms of the films used for ATR-SEIRAS (Figure S7) confirm that their electrochemical properties are the same as those of the Au foil used for chromatographic analysis. The applied potential was stepped down from 0.58 to −1.02 V and the spectrum taken at 0.58 V was used as the background for the experiments in 0.07 $KHCO_3$. For the experiments in 0.07 $KHCO_3$ with 15 mol % DMF, the applied potential was stepped down from 0.63 to −0.97 V, and the spectrum taken at 0.63 V was used as the background.

According to previous studies,[34] the O−H stretching mode of H_2O can be deconvoluted into three peaks corresponding to ice-like water with four H-bonds at ∼3250 cm^{-1}, asymmetric H-bonded water having one to three H-bonds at ∼3400 cm^{-1}, and water molecules with a very low degree of H-bonding (most likely H-accepting and not H-donating molecules) at ∼3600 cm^{-1}. Although Bonn and co-workers[35] have shown that the shape of the O−H stretching band of interfacial water is due to a Fermi resonance of the symmetric stretching with the overtone of the water bending, the same group[36] have shown that, although this intramolecular vibrational coupling is responsible for the shape of the band, it still holds true that hydrogen bonding between water molecules provokes a red shift of the O−H stretching. We will therefore base our analysis on this hydrogen bonding-induced red shift and avoid assigning specific components of the O−H stretching band to specific vibrational modes.

In CO_2-saturated and DMF-free $KHCO_3$ (Figure 2A), the intensity of the ν-OH band increases and slowly red-shifts with increasingly negative potential. As shown by the deconvoluted spectra, this apparent red shift is the result of a change in the weight of the different components of the O−H stretching envelope. Osawa and co-workers[37] interpreted the changes in the O−H region of the spectrum as due to changes in the degree of hydrogen bonding due to the potential-induced reorientation of interfacial water. Although water reorientation is certainly responsible for the observed potential-induced spectral changes, the association between these and a change of the degree of hydrogen bonding might need to be revisited. This, however, is out of the scope of this manuscript and will be dealt with elsewhere.

When DMF is present (Figure 2B), negative absorption peaks appear around 2850−2920 cm^{-1} when the potential is made more negative than that of the background at 0.63 V, which must be interpreted as both the CH_3 and H−CO stretching modes of DMF becoming more parallel to the electrode surface. This could be due either to the reorientation of interfacial DMF or to the exclusion of DMF from the interface at negative potentials. The shape of the carbonyl band of DMF (Figure 2C), with a negative and a positive lobe, is strong evidence, however, that reorientation and not exclusion of DMF from the double layer must be responsible for the negative bands around 2850−2920 cm^{-1}. However, due to interference of the water bending mode around 1645 cm^{-1} as discussed above, experiments in D_2O are needed to analyze the potential dependence of the DMF bands in the carbonyl region. Figure 2C shows potential-dependent ATR-SEIRA spectra in 15 mol % DMF in 0.07 M $KHCO_3$ in D_2O. Negative and positive absorption peaks appeared at 1715 and 1655 cm^{-1}, respectively. Although the intensity of both peaks increased with increasing negative potential, the negative peak at 1715 cm^{-1} is clearly more intense than the positive peak at 1655 cm^{-1}. These frequencies are characteristic of carbonyl groups and both of them must therefore be assigned to the C═O stretching of interfacial DMF. The positive band at 1655 cm^{-1} coincides in fact almost exactly with that of bulk DMF in 15 mol % solutions in D_2O (Figure 1E and black line in the spectra on top of panel (C) in Figure 2), but the frequency of the negative band at 1715 cm^{-1} is even higher than that of the C═O stretching in pure DMF (Figure 1D,E and red line in the spectra on top of panel (C) in Figure 2). As we discussed previously, hydrogen bonding between water and the oxygen atom of the carbonyl group of DMF results in a red shift of the carbonyl stretching band. The negative absorption band at 1715 cm^{-1} can therefore be attributed to DMF molecules with their C═O group pointing toward the electrode surface, which can therefore not form any hydrogen bond at all with either water molecules or other DMF molecules. As the applied potential is made increasingly negative, the oxygen atom of DMF will be pushed away from the negatively charged electrode surface, which will favor the formation of hydrogen bonds with water and will red-shift the C═O stretching frequency of the carbonyl group. The larger intensity of the negative band at 1715 cm^{-1} suggests that, at the potential at which the background had been recorded (0.63 V), the C═O bond pointing toward the electrode was more perpendicular to the surface than when pointing away from the surface. This picture is consistent with both the lone pairs of the O and the N atoms being pushed away from the surface by the electric field. The potential dependence of the integrated intensity of the DMF band just below 1400 cm^{-1} is also consistent with this potential-induced reorientation of interfacial DMF.

The positive band at 1620 cm^{-1} in Figure 2E belongs to bicarbonate.[38] Although anions can be expected to be expelled from the interface when the potential is stepped negatively, both the CO2RR and the HER result in an increase of the pH at the interface, which will increase the interfacial concentration of bicarbonate due to the resulting shift in the CO_2/HCO_3^- equilibrium toward the latter.[38]

Contrary to what was observed for the bulk of the solution (Figure 1), the shape of the OH-stretching band of interfacial water is quite different in the presence of 15 mol % of DMF (Figure 2B), which by itself is a clear indication that DMF affects the structure of interfacial water. The intensity of the band is also comparatively smaller as expected due to the lower concentration of water in the system. The different effect of DMF on the structures of bulk and interfacial water suggests a positive surface excess of DMF at the interface.

https://doi.org/10.1021/acscatal.3c01223
ACS Catal. 2023, 13, 8384−8393

The difference between the OH-stretching bands in the presence and absence of DMF is partly due to changes in the relative contributions of the components of the broad O−H stretching band at 3245, 3400, and 3600 cm^{-1} (the relative weights of the former and the latter increase in the presence of DMF). The deconvolution of the water OH-stretching band with and without DMF is presented in Figure 2D,E, respectively. The deconvolution of the band with 15 mol % DMF (Figure 2E) reveals an additional peak at 3000 cm^{-1}, also clearly seen as a shoulder in Figure 2B. The graph in Figure 2F clearly shows that the additional peak at 3000 cm^{-1} appears in parallel to the disappearance of non-H-bonded C═O and nearly in parallel to the appearance of H-bonded C═O. This strongly suggests that the water responsible for this new contribution is precisely that hydrogen bonded to DMF and that the potential-induced reorientation of interfacial DMF (maybe also the reorientation of interfacial water itself) plays a role in allowing this to happen. Also, the plateauing of the intensity of the band at 3000 cm^{-1} coupled with the decrease in the band at 1655 cm^{-1} at very negative potentials might be a sign of H-bonding to the N atom of DMF. Hence, we attribute this additional water band at 3000 cm^{-1} to water molecules, which are strongly H-bonded to DMF. The deconvolution of all of the water OH bending bands at different potentials and the evolution of each of the resulting contributions with potential is shown in Figure S9. A significant feature we observe in Figure 2F is that all of the bands either plateau or decrease in intensity around 0.6 V, where the maximum CO2RR FE was seen. This correlation between the band intensities and the maximum CO FE adds support to our main conclusion that the structure of interfacial water and the effect thereupon of adding DMF has a direct impact on the FE.

Another interesting feature in the OH-stretching band in the presence of DMF is the higher intensity of the band centered at 3600 cm^{-1}, as compared with the spectra in the absence of DMF. A band at 3610 cm^{-1} has been observed in the bulk of water−ionic liquid mixtures[39] and was attributed to water molecules with a low degree of hydrogen bonding within a water-in-salt environment. It was suggested later that these water molecules contribute to stabilizing the CO_2^- radical formed after the first electron transfer to CO_2 in the CO2RR, thereby leading to enhanced activity for the CO2RR in these ionic liquid−water mixtures.[17] It is reasonable to also attribute the OH-stretching contribution at 3600 cm^{-1} to interfacial water molecules with a low degree of hydrogen bonding within a DMF-rich environment, although we have no evidence in this case of enhanced activity for the CO2RR induced by these water molecules.

The accumulation of DMF at the interface suggested by the difference between the bulk and interfacial spectra of solutions containing 15 mol % DMF must be responsible for the increased contribution of these interfacial water molecules at all potentials, as compared with DMF-free electrolytes. The potential dependence of this contribution to the O−H stretching band of water, which runs in parallel with the negative band at 1715 cm^{-1} is consistent with this interpretation: as the lone pairs of the O and N atoms of DMF are pushed away from the electrode (allowing for increased hydrogen bonding with molecules in the second interfacial layer and leading to an increase of the intensity of the component around 3000 cm^{-1}, as discussed above), the water molecules closer to the electrode surface will now be able to hydrogen-bond to DMF. The interfacial electrolyte structure modifications with the addition of DMF molecules is summarized in the form of a schematic cartoon in Figure 3.

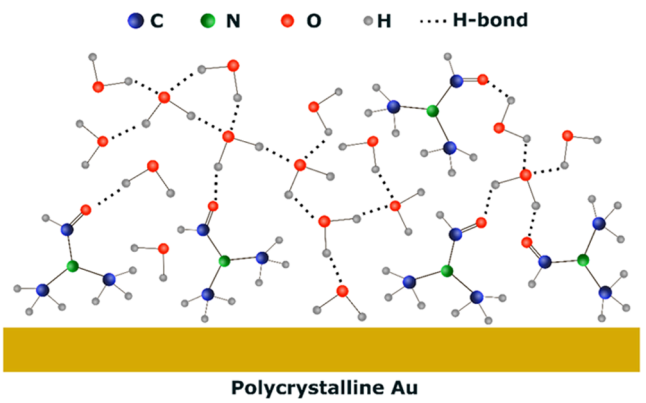

Figure 3. Schematic illustration of the modification of the interfacial structure in the presence of DMF in the electrolyte.

The H−O−H bending mode of water can also provide crucial information about the water structure.[40] However, the overlap of this mode with the C═O stretching mode of DMF in H_2O solutions and with the asymmetric N−CH_3 stretching of DMF in D_2O solutions prevents a thorough analysis. We note nonetheless that the D−O−D bending band is much broader in the presence of DMF (Figure S8), which suggests the presence of different contributions originating from different water environments.

CO adsorbed on Au (CO_{ad}), an obvious reaction intermediate in the reaction of CO_2 to CO, could be detected in CO_2-saturated 0.07 M $KHCO_3$ both in the presence and in the absence of DMF (Figure 4A,B) as a band with frequency between 2090 and 2120 cm^{-1}, consistent with assignments to linearly bonded CO_{ad} in previous work.[41−44] This assignment is confirmed by comparing the peak in Figure 4A,B with that in Figure 4D, obtained when CO is adsorbed directly on Au from a CO-saturated solution. The red shift of the CO_{ad} with increasingly negative electrode potential is due to the well-known electrochemical Stark effect.[45−48] Figure 4E−G shows that the Stark tuning rate is similar (around 30 cm^{-1} V^{-1}) in all three cases (CO_2-saturated DMF-free 0.07 M $KHCO_3$, CO_2-saturated DMF-containing 0.07 M $KHCO_3$, and CO-saturated DMF-containing 0.07 M $KHCO_3$), adding further support to our assignment to CO_{ad}. The intensity of the band is weaker in the absence of DMF, which is consistent with the lower Faradaic efficiency in this case, in which CO_{ad} was only observed between 0.38 and −0.22 V. No bands could be detected within this potential region in the frequency region characteristic of bridge-bonded CO_{ad}. A very weak and broad feature appears however just above 1800 cm^{-1} at potentials more negative than −0.62 V. We will discuss this band below when analyzing the data in DMF-containing CO_2-saturated 0.07 M $KHCO_3$.

Interestingly, the band in Figure 4A,B that we have assigned to linearly bonded CO_{ad} has a clear bipolar character. However, as shown in Figure 4C, when the background is collected at 1.03 instead of 0.63 V, the bipolar feature around 2100 cm^{-1} is substituted by two positive bands. The band at higher frequency (~2150 cm^{-1}) appears at 0.83 V and its intensity first increases up to 0.43 V with a Stark tuning rate of 20 cm^{-1} V^{-1} and then remains approximately constant. From 0.23 V a new peak appears at ~2110 cm^{-1} whose frequency

https://doi.org/10.1021/acscatal.3c01223
ACS Catal. 2023, 13, 8384−8393

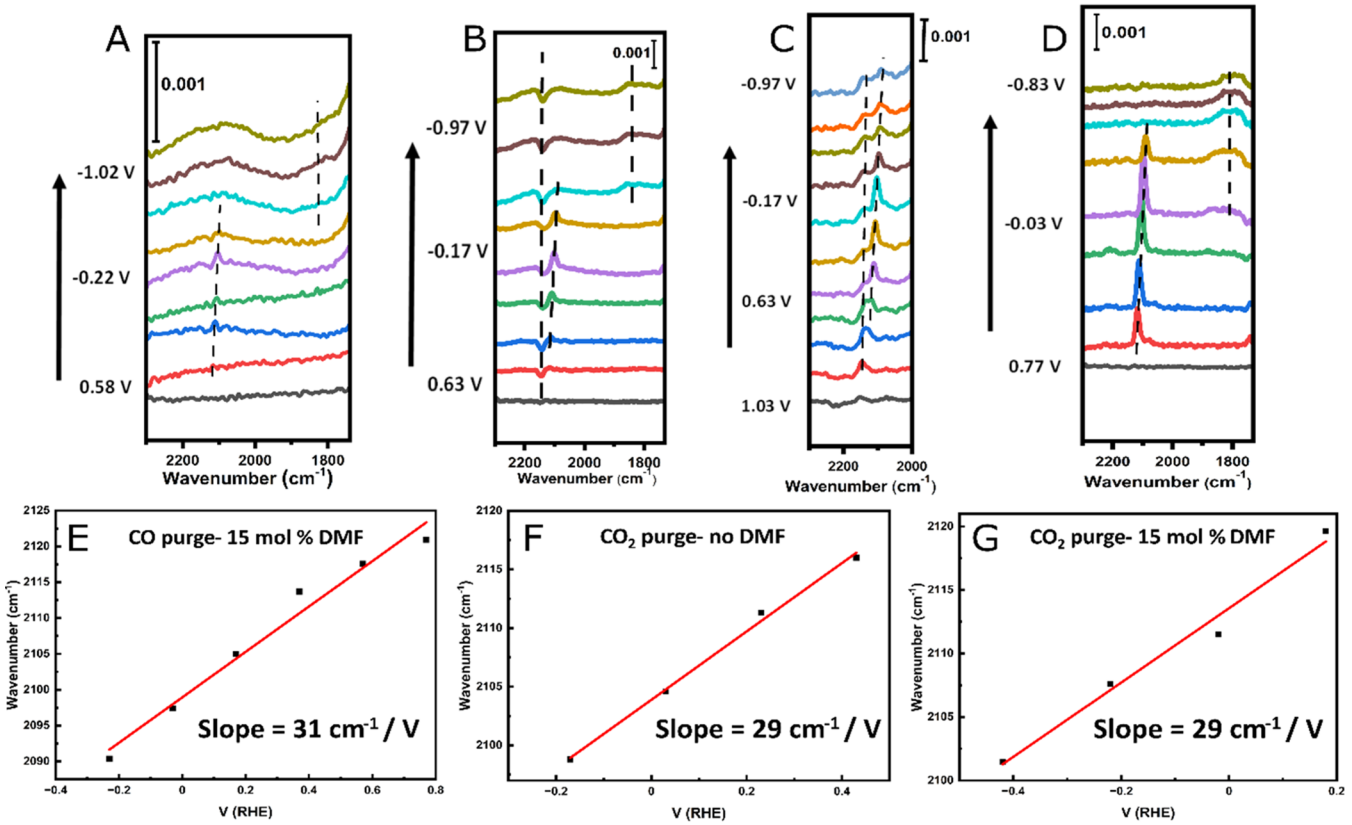

Figure 4. Potential-dependent *in situ* ATR-SEIRA spectra of Au in the spectral region between 1750 and 2300 cm^{-1} in CO_2-saturated 0.07 M $KHCO_3$ (A) and in CO_2 saturated 15 mol % DMF in 0.07 M $KHCO_3$ (B, C). The background spectrum was collected at 0.58 V in (A), at 0.63 V in (B), and at 1.03 V in (C). Potential-dependent *in situ* ATR-SEIRA spectra of Au in CO-saturated 15 mol % DMF in 0.07 M $KHCO_3$ are shown in (D). The background spectrum in (D) was collected before saturating the solution with CO. The Stark shift of CO adsorbed on Au is also presented when CO_{ad} is adsorbed directly from CO-saturated 15 mol % DMF in 0.07 M $KHCO_3$ (E), when CO_{ad} is formed by the reduction of CO_2 in CO_2-saturated 0.07 M $KHCO_3$ (F) and when CO_{ad} is formed by the reduction of CO_2 in CO_2-saturated 15 mol % DMF in 0.07 M $KHCO_3$ (G).

shifts with a Stark tuning rate of 29 cm^{-1} V^{-1} and whose intensity first increases and then decreases, just exactly as the bands at this frequency in Figure 4B,D. Although, arguably 2150 cm^{-1} is too high a frequency for CO_{ad}, in order to explore if adsorption of CO on different surface sites might be responsible for the presence of two bands around and above 2100 cm^{-1}, we recorded ATR-SEIRA spectra of CO adsorbed directly on Au from the solution by saturating the electrolyte with CO (Figure 4D). This results in a single positive peak around 2100 cm^{-1}, with a similar Stark shift (31 cm^{-1} V^{-1}), as those observed at the same frequency in both DMF-free and DMF-containing CO_2-saturated 0.07 M $KHCO_3$ (Figure 4E). Surprisingly, this peak is very symmetric and appears at the same frequency, if the same potential is compared, as the clearly smaller CO_{ad} bands obtained by reducing CO_2 in DMF-containing CO_2-saturated 0.07 M $KHCO_3$ (Figure 4B). Dipole−dipole coupling between neighboring CO_{ad} oscillators should lead to an increase in the stretching frequency and, if different sites are occupied, dipole−dipole coupling should also lead to intensity stealing in favor of those oscillators with a higher resonance frequency, which results in inhomogeneous broadening of the absorption bands of adsorbed species. The absence of both these features suggests that, even when CO is adsorbed directly from the solution, the coverage is relatively low and only one type of adsorption sites is being occupied (most likely those sites where CO adsorption is stronger, not necessarily the same where the reaction takes place).

The region between 2000 and 2200 cm^{-1} is a very clean spectral region where very few functional groups have bands, essentially only CN in cyanides and CO in carbon monoxide. Trisler et al.[49] reported the presence of HCN at concentrations ~10^{-4} M in DMF distilled over CaH_2 in natural light. This makes the attribution of the band at ~2150 cm^{-1} to adsorbed cyanide tempting. In addition, the Stark tuning rate of 20 cm^{-1} V^{-1} is comparable to that reported for the Au−CN band.[50] The peak at ~2150 cm^{-1} also appears in ATR-SEIRA spectra of the Au electrode in N_2-saturated 15 mol % DMF in 0.07 M $KHCO_3$ (Figure S10), which strongly suggests that the band must correspond to either cyanide generated by decomposition of DMF or to an impurity present in DMF containing a nitrile functionality.

Figure 4B,D (and to a lesser extent, also Figure 4A) also contains a broad band appearing around ~1800 cm^{-1} at the negative potential end of the experiments. This band starts to appear below −0.43 V in CO-saturated solutions and at around −0.57 V in CO_2-saturated solutions (Figure 4A,B), although it is much weaker in DMF-free 0.07 M $KHCO_3$ (Figure 4A). We assign this band to bridge-bonded CO_{ad}, which forms due to a change in the adsorption mode of CO_{ad} at very negative potentials, by which linearly bonded transforms into bridge-bonded CO_{ad}. A similar effect is known for CO_{ad} on Pt electrodes.[51,52]

https://doi.org/10.1021/acscatal.3c01223
ACS Catal. 2023, 13, 8384−8393

4. CONCLUSIONS

In summary, we have shown that 15 mol % of *N*,*N*-dimethylformamide (DMF) as an electrolyte additive can boost the Faradaic efficiency (FE) of electrochemical CO_2 reduction reaction (CO2RR) to ∼94% on polycrystalline gold electrodes.

Using potential-dependent *in situ* ATR-SEIRAS, we have been able to show that accumulation of DMF at the interface modifies the structure of interfacial water, yielding a new kind of water species with strong H-bonding to the O and possibly also the N atoms of DMF. The emergence of the new contribution to the OH-stretching band of water at 3000 cm^{-1} (due to the new water environment) and the change in the relative weight of the other components of the band strongly indicate that the effect of DMF is not to simply displace water from the interface. By comparing the potential dependence of the FE in the absence and presence of DMF with the evolution of the different contributions to the O−H stretching of interfacial water, we conclude that both exclusion of water from the interface and the DMF-induced changes in the structure of interfacial water must contribute to inhibiting the hydrogen evolution reaction (HER) and therefore increasing the FE for CO when reducing CO_2. Besides, we also observed that this HER suppression strategy is not limited to our system of study and is also effective even with platinum, the best single-element catalyst known for the HER. Linearly bonded adsorbed CO, which was substituted by bridge-bonded adsorbed CO at the most negative potentials explored, was detected during the CO2RR by *in situ* ATR-SEIRAS.

Based on these results, we have successfully demonstrated that the FE of the CO2RR can be increased through a combination of decreasing the chemical potential of water at the interface and manipulating the H-bonding network of interfacial water with the addition of DMF. Our study stresses the importance of simple and efficient electrolyte engineering methods for electrocatalysis applications and how applying highly sensitive spectroscopic techniques can help us get a deeper understanding of the different interfacial phenomena that can affect the electrocatalytic properties of a given system.

■ ASSOCIATED CONTENT

Supporting Information

The Supporting Information is available free of charge at https://pubs.acs.org/doi/10.1021/acscatal.3c01223.

Experimental methods, starting materials, preparation of Au film on silicon prism, electrochemical measurements, gas chromatography, additional electrochemical data, ^1H NMR spectroscopy data, SEM data, EDS data, spectro-electrochemical setup, and ATR-SEIRA spectra under N_2-saturated conditions (PDF)

■ AUTHOR INFORMATION

Corresponding Authors

Tharangattu N. Narayanan − *Tata Institute of Fundamental Research Hyderabad, Hyderabad 500046, India;* orcid.org/0000-0002-5201-7539; Email: tnn@tifrh.res.in

Angel Cuesta − *School of Natural and Computing Sciences, University of Aberdeen, AB24 3UE Aberdeen, Scotland, U.K.; Centre for Energy Transition, University of Aberdeen, AB24 3FX Aberdeen, Scotland, U.K.;* orcid.org/0000-0003-4243-1848; Email: angel.cuestaciscar@abdn.ac.uk

Author

Nandita Mohandas − *Tata Institute of Fundamental Research Hyderabad, Hyderabad 500046, India; School of Natural and Computing Sciences, University of Aberdeen, AB24 3UE Aberdeen, Scotland, U.K.*

Complete contact information is available at: https://pubs.acs.org/10.1021/acscatal.3c01223

Author Contributions

N.M. and T.N.N. conceived the idea. All of the ATR-SEIRAS experiments were designed by A.C., and the spectra were analyzed by A.C. and N.M. All of the experiments were performed by N.M. All authors participated in the data analyses, and the manuscript was written through the contributions of all authors.

Notes

The authors declare no competing financial interest.

■ ACKNOWLEDGMENTS

N.M. and T.N.N. acknowledge the support of the Department of Atomic Energy, Government of India, under Project Identification No. RTI4007. N.M. acknowledges the funding support of Infosys Foundation through Infosys—TIFR Leading Edge Travel Grant. N.M. acknowledges Dr. Anku Guha and Dr. Andrew Burley for useful discussions. A.C. acknowledges the continued support of the University of Aberdeen.

■ REFERENCES

(1) Golru, S. S.; Biddinger, E. J. Effect of Additives in Aqueous Electrolytes on CO_2 Electroreduction. *Chem. Eng. J.* **2022**, *428*, No. 131303.

(2) König, M.; Vaes, J.; Klemm, E.; Pant, D. Solvents and Supporting Electrolytes in the Electrocatalytic Reduction of CO_2. *iScience* **2019**, *19*, 135−160.

(3) Gao, D.; Arán-Ais, R. M.; Jeon, H. S.; Cuenya, B. R. Rational Catalyst and Electrolyte Design for CO2 Electroreduction towards Multicarbon Products. *Nat. Catal.* **2019**, *2*, 198−210.

(4) Nitopi, S.; Bertheussen, E.; Scott, S. B.; Liu, X.; Engstfeld, A. K.; Horch, S.; Seger, B.; Stephens, I. E. L.; Chan, K.; Hahn, C.; et al. Progress and Perspectives of Electrochemical CO_2 Reduction on Copper in Aqueous Electrolyte. *Chem. Rev.* **2019**, *119*, 7610−7672.

(5) Saha, P.; Amanullah, S.; Dey, A. Selectivity in Electrochemical CO_2 Reduction. *Acc. Chem. Res.* **2022**, *55*, 134−144.

(6) Nam, D.-H.; de Luna, P.; Rosas-Hernández, A.; Thevenon, A.; Li, F.; Agapie, T.; Peters, J. C.; Shekhah, O.; Eddaoudi, M.; Sargent, E. H. Molecular Enhancement of Heterogeneous CO_2 Reduction. *Nat. Mater.* **2020**, *19*, 266−276.

(7) Dattila, F.; Seemakurthi, R. R.; Zhou, Y.; López, N. Modeling Operando Electrochemical CO_2 Reduction. *Chem. Rev.* **2022**, *122*, 11085−11130.

(8) Cave, E. R.; Montoya, J. H.; Kuhl, K. P.; Abram, D. N.; Hatsukade, T.; Shi, C.; Hahn, C.; Nørskov, J. K.; Jaramillo, T. F. Electrochemical CO_2 Reduction on Au Surfaces: Mechanistic Aspects Regarding the Formation of Major and Minor Products. *Phys. Chem. Chem. Phys.* **2017**, *19*, 15856−15863.

(9) Goyal, A.; Marcandalli, G.; Mints, V. A.; Koper, M. T. M. Competition between CO_2 Reduction and Hydrogen Evolution on a Gold Electrode under Well-Defined Mass Transport Conditions. *J. Am. Chem. Soc.* **2020**, *142*, 4154−4161.

(10) Hori, Y.; Murata, A.; Kikuchi, K.; Suzuki, S. Electrochemical Reduction of Carbon Dioxides to Carbon Monoxide at a Gold Electrode in Aqueous Potassium Hydrogen Carbonate. *J. Chem. Soc., Chem. Commun.* **1987**, 728−729.

(11) de Salles Pupo, M. M.; Kortlever, R. Electrolyte Effects on the Electrochemical Reduction of CO_2. *ChemPhysChem* **2019**, *20*, 2926−2935.
(12) Thevenon, A.; Rosas-Hernández, A.; Peters, J.; Agapie, T. In Situ Nanostructuring and Stabilization of Polycrystalline Copper Electrodes with Organic Salt Additives Promotes CO_2 Reduction to Ethylene. *Angew. Chem., Int. Ed.* **2019**, *58*, 16952−16958.
(13) Zhang, Z.-Q.; Banerjee, S.; Thoi, V. S.; Shoji Hall, A. Reorganization of Interfacial Water by an Amphiphilic Cationic Surfactant Promotes CO_2 Reduction. *J. Phys. Chem. Lett.* **2020**, *11*, 5457−5463.
(14) Banerjee, S.; Han, X.; Thoi, V. S. Modulating the Electrode−Electrolyte Interface with Cationic Surfactants in Carbon Dioxide Reduction. *ACS Catal.* **2019**, *9*, 5631−5637.
(15) Ge, W.; Chen, Y.; Fan, Y.; Zhu, Y.; Liu, H.; Song, L.; Liu, Z.; Lian, C.; Jiang, H.; Li, C. Dynamically Formed Surfactant Assembly at the Electrified Electrode−Electrolyte Interface Boosting CO_2 Electroreduction. *J. Am. Chem. Soc.* **2022**, *144*, 6613−6622.
(16) Neubauer, S. S.; Krause, R. K.; Schmid, B.; Guldi, D. M.; Schmid, G. Overpotentials and Faraday Efficiencies in CO_2 Electrocatalysis−the Impact of 1-Ethyl-3-Methylimidazolium Trifluoromethanesulfonate. *Adv. Energy Mater.* **2016**, *6*, No. 1502231.
(17) Yang, X.-H.; Papasizza, M.; Cuesta, A.; Cheng, J. Water-In-Salt Environment Reduces the Overpotential for Reduction of CO_2 to CO_2^- in Ionic Liquid/Water Mixtures. *ACS Catal.* **2022**, *12*, 6770−6780.
(18) Golru, S. S.; Biddinger, E. J. Effect of Anion in Diluted Imidazolium-Based Ionic Liquid/Buffer Electrolytes for CO_2 Electroreduction on Copper. *Electrochim. Acta* **2020**, *361*, No. 136787.
(19) Dong, Q.; Zhang, X.; He, D.; Lang, C.; Wang, D. Role of H_2O in CO_2 Electrochemical Reduction as Studied in a Water-in-Salt System. *ACS Cent. Sci.* **2019**, *5*, 1461−1467.
(20) Abdinejad, M.; Mirza, Z.; Zhang, X.; Kraatz, H.-B. Enhanced Electrocatalytic Activity of Primary Amines for CO_2 Reduction Using Copper Electrodes in Aqueous Solution. *ACS Sustainable Chem. Eng.* **2020**, *8*, 1715−1720.
(21) Morris, A. J.; McGibbon, R. T.; Bocarsly, A. B. Electrocatalytic Carbon Dioxide Activation: The Rate-determining Step of Pyridinium-catalyzed CO2 Reduction. *ChemSusChem* **2011**, *4*, 191−196.
(22) Albo, J.; Beobide, G.; Castaño, P.; Irabien, A. Methanol Electrosynthesis from CO_2 at Cu_2O/ZnO Prompted by Pyridine-Based Aqueous Solutions. *J. CO_2 Util.* **2017**, *18*, 164−17282.
(23) Yang, B.; Lang, H.; Liu, Z.; Wang, S.; Men, Z.; Sun, C. Three Stages of Hydrogen Bonding Network in DMF-Water Binary Solution. *J. Mol. Liq.* **2021**, *324*, No. 114996.
(24) Wang, J.; Gao, W.; Zhong, H.; Liang, C.; Chen, X.; Lüdemann, H.-D.; Chen, L. A Systematic Study on the Intradiffusion and Structure of N,N-Dimethylformamide−Water Mixtures: By Experiment and Molecular Dynamics Simulation. *RSC Adv.* **2016**, *6*, 85603−85611.
(25) Yuan, X.; Li, Y.; Zhu, Y.; Deng, W.; Li, C.; Zhou, Z.; Hu, J.; Zhang, M.; Chen, H.; Li, R. Low Concentration DMF/H_2O Hybrid Electrolyte: A New Opportunity for Anode Materials in Aqueous Potassium-Ion Batteries. *ACS Appl. Mater. Interfaces* **2021**, *13*, 38248−38255.
(26) Ma, Y.; Zhang, Q.; Liu, L.; Li, Y.; Li, H.; Yan, Z.; Chen, J. N, N-Dimethylformamide Tailors Solvent Effect to Boost Zn Anode Reversibility in Aqueous Electrolyte. *Natl. Sci. Rev.* **2022**, *9*, No. nwac051.
(27) Cuesta, A. ATR-SEIRAS for Time-Resolved Studies of Electrode−Electrolyte Interfaces. *Curr. Opin. Electrochem.* **2022**, *35*, No. 101041.
(28) Guha, A.; Sahoo, M.; Alam, K.; Rao, D. K.; Sen, P.; Narayanan, T. N. Role of Water Structure in Alkaline Water Electrolysis. *iScience* **2022**, *25*, No. 104835.
(29) Durgaprasad, G.; Sathyanarayana, D. N.; Patel, C. C. Infrared Spectra and Normal Vibrations of N, N-Dimethylformamide and N, N-Dimethylthioformamide. *Bull. Chem. Soc. Jpn.* **1971**, *44*, 316−322.
(30) Zhu, S.; Li, T.; Cai, W.-B.; Shao, M. CO_2 Electrochemical Reduction As Probed through Infrared Spectroscopy. *ACS Energy Lett.* **2019**, *4*, 682−689.
(31) Cuesta, A. Composition, Structure, and Reaction Dynamics at Electrode−Electrolyte Interfaces Using Infrared Spectroscopy. In *Vibrational Spectroscopy at Electrified Interfaces*, 1st ed.; Wieckowski, A.; Korzeniewski, C.; Braunschweig, B., Eds.; John Wiley & Sons, Inc., 2013; Chapter 8, pp 266−306.
(32) Cuesta, A. Towards a Molecular Level Understanding of Electrochemical Interfaces and Electrocatalytic Reactions. *Johnson Matthey Technol. Rev.* **2014**, *58*, 202−204.
(33) Kas, R.; Ayemoba, O.; Firet, N. J.; Middelkoop, J.; Smith, W. A.; Cuesta, A. In-situ Infrared Spectroscopy Applied to the Study of the Electrocatalytic Reduction of CO_2: Theory, Practice and Challenges. *ChemPhysChem* **2019**, *20*, 2904−2925.
(34) Rao, R. R.; Huang, B.; Katayama, Y.; Hwang, J.; Kawaguchi, T.; Lunger, J. R.; Peng, J.; Zhang, Y.; Morinaga, A.; Zhou, H.; You, H.; Shao-Horn, Y. PH- and Cation-Dependent Water Oxidation on Rutile RuO_2(110). *J. Phys. Chem. C* **2021**, *125*, 8195−8207.
(35) Schaefer, J.; Backus, E. H. G.; Nagata, Y.; Bonn, M. Both Inter- and Intramolecular Coupling of O−H Groups Determine the Vibrational Response of the Water/Air Interface. *J. Phys. Chem. Lett.* **2016**, *7*, 4591−4595.
(36) Sovago, M.; Campen, R. K.; Wurpel, G. W.; Müller, M.; Bakker, H. J.; Bonn, M. Vibrational response of hydrogen-bonded interfacial water is dominated by intramolecular coupling. *Phys. Rev. Lett.* **2008**, *100*, No. 173901.
(37) Ataka, K.-i.; Yotsuyanagi, T.; Osawa, M. Potential-Dependent Reorientation of Water Molecules at an Electrode/Electrolyte Interface Studied by Surface-Enhanced Infrared Absorption Spectroscopy. *J. Phys. Chem. A* **1996**, *100*, 10664−10672.
(38) Ayemoba, O.; Cuesta, A. Spectroscopic Evidence of Size-Dependent Buffering of Interfacial pH by Cation Hydrolysis during CO_2 Electroreduction. *ACS Appl. Mater. Interfaces* **2017**, *9*, 27377−27382.
(39) Papasizza, M.; Cuesta, A. In Situ Monitoring Using ATR-SEIRAS of the Electrocatalytic Reduction of CO_2 on Au in an Ionic Liquid/Water Mixture. *ACS Catal.* **2018**, *8*, 6345−6352.
(40) Seki, T.; Chiang, K.-Y.; Yu, C.-C.; Yu, X.; Okuno, M.; Hunger, J.; Nagata, Y.; Bonn, M. The Bending Mode of Water: A Powerful Probe for Hydrogen Bond Structure of Aqueous System. *J. Phys. Chem. Lett.* **2020**, *11*, 8459−8469.
(41) Dunwell, M.; Lu, Q.; Heyes, J. M.; Rosen, J.; Chen, J. G.; Yan, Y.; Jiao, F.; Xu, B. The Central Role of Bicarbonate in the Electrochemical Reduction of Carbon Dioxide on Gold. *J. Am. Chem. Soc.* **2017**, *139*, 3774−3783.
(42) Miyake, H.; Ye, S.; Osawa, M. Electroless Deposition of Gold Thin Films on Silicon for Surface-Enhanced Infrared Spectroelectrochemistry. *Electrochem. Commun.* **2002**, *4*, 973−977.
(43) Sun, S.-G.; Cai, W.-B.; Wan, L.-J.; Osawa, M. Infrared Absorption Enhancement for CO Adsorbed on Au Films in Perchloric Acid Solutions and Effects of Surface Structure Studied by Cyclic Voltammetry, Scanning Tunneling Microscopy, and Surface-Enhanced IR Spectroscopy. *J. Phys. Chem. B* **1999**, *103*, 2460−2466.
(44) Pronkin, S.; Hara, M.; Wandlowski, T. Electrocatalytic Properties of Au(111)-Pd Quasi-Single-Crystal Film Electrodes as Probed by ATR-SEIRAS. *Russ. J. Electrochem.* **2006**, *42*, 1177−1192.
(45) Pons, S.; Korzeniewski, C.; Shirts, R. B.; Bewicks, A. Field-Induced Infrared Absorption in Metal Surface Spectroscopy: The Electrochemical Stark Effect. *J. Phys. Chem. A* **1985**, *89*, 2297−2298.
(46) Lambert, D. K. Stark Effect of Adsorbate Vibrations. *Solid State Commun.* **1984**, *51*, 297−300.
(47) Lambert, D. K. Vibrational Stark Effect of Adsorbates at Electrochemical Interfaces. *Electrochim. Acta* **1996**, *41*, 623−630.
(48) Wuttig, A.; Yaguchi, M.; Motobayashi, K.; Osawa, M.; Surendranath, Y. Inhibited Proton Transfer Enhances Au-Catalyzed CO_2-to-Fuels Selectivity. *Proc. Natl. Acad. Sci. U.S.A.* **2016**, *113*, E4585−E4593.

https://doi.org/10.1021/acscatal.3c01223
ACS Catal. 2023, 13, 8384−8393

(49) Trisler, J. C.; Freasier, B. F.; Wu, S.-M. The Detection of Hydrogen Cyanide Present as an Impurity in n,n-Dimethyformamide. *Tetrahedron Lett.* **1974**, *15*, 687−690.
(50) Ge, A.; Videla, P. E.; Lee, G. L.; Rudshteyn, B.; Song, J.; Kubiak, C. P.; Batista, V. S.; Lian, T. Interfacial Structure and Electric Field Probed by in Situ Electrochemical Vibrational Stark Effect Spectroscopy and Computational Modeling. *J. Phys. Chem. C* **2017**, *121*, 18674−18682.
(51) Roth, J. D.; Weaver, M. J. Role of Double-Layer Cation on the Potential-Dependent Stretching Frequencies and Binding Geometries of Carbon Monoxide at Platinum-Nonaqueous Interfaces. *Langmuir* **1992**, *8*, 1451−1458.
(52) Hussain, G.; Pérez-Martínez, L.; Le, J.-B.; Papasizza, M.; Cabello, G.; Cheng, J.; Cuesta, A. How Cations Determine the Interfacial Potential Profile: Relevance for the CO_2 Reduction Reaction. *Electrochim. Acta* **2019**, *327*, No. 135055.

https://doi.org/10.1021/acscatal.3c01223
ACS Catal. 2023, 13, 8384−8393